LIGO SCIENTIFIC COLLABORATION
VIRGO COLLABORATION

Document Type	**LIGO-T1100093-v2**	August 27, 2013

Gravitational Wave Emission from Accretion Disk Instabilities – Analytic Models

Lucía Santamaría (LIGO Lab, Caltech, luciasan@caltech.edu),
Christian D. Ott (TAPIR/CaRT, Caltech, cott@tapir.caltech.edu)

Abstract

We derive the gravitational wave emission from accretion disk instabilities in long gamma-ray bursts or black-hole forming core-collapse supernovae based on simple analytic models of van Putten and Piro & Pfahl.

WWW: http://www.ligo.org/ and http://www.virgo.infn.it

Processed with LaTeX on 2013/08/31

1 Introduction

We derive analytic estimates for the gravitational wave (GW) emission from the following analytic accretion disk instability models in the context of Collapsar-type gamma-ray bursts and black-hole (BH) forming core-collapse supernovae:

- **The suspended-accretion-driven disk instability proposed by van Putten** [1, 2].
  In this instability, turbulence in a thick accretion torus is driven by strong coupling between the torus and the ergosphere of the central BH by MHD effects. In this picture, the quadrupole components of the disk turbulence lead to GW emission that (via the strong coupling) spin down the BH. The strong coupling and the energetics of the associated GW emission proposed by van Putten are generally regarded as too optimistic (possibly by orders of magnitude). Nevertheless, we include this model, since it makes useful, falsifiable predictions.

  We advise that authors wishing to use the waveforms predicted by our ad-hoc version of van Putten's model state clearly to their readers that it is unlikely that a realistic accretion disk instability will produce a gravitational wave signal of the kind predicted by the model implemented here.

- **Collapsar Disk Fragmentation by Piro & Pfahl** [3].
  Gravitational instability causes fragmentation of the massive accretion disk within a collapsing, rotating star. This fragment spirals into the newly-formed BH at the center of the accretion disk due to a combination of disk viscosity and GW emission, producing a unique GW signature.

In the following, we work in physical units, including all relevant factors of the gravitational constant G and of the speed of light c. Accompanying this technical report are two python scripts, `vanPuttengw.py` and `pirogw.py`, that implement the models described here and provide both GW polarizations as output.

2 Suspended-Accretion Quadrupole Disk Instability

Following along the lines of van Putten's ideas, we assume a spinning Kerr BH with dimensionless Kerr spin parameter $a^\star = (c/G)J_{\rm BH}/M_{\rm BH}^2$ ($0 \leq a^\star < 1$) with an accretion disk/torus of mass $M_{\rm disk}$. The disk extends to the radius of the innermost stable orbit [4],

$$R_{\rm ISCO} = \left(\frac{G}{c^2}\right) M_{\rm BH} \left(3 + Z_2 \mp \left[(3-Z_1)(3+Z_1+2Z_2)\right]^{1/2}\right), \tag{1}$$

$$Z_1 = 1 + (1-a^{\star 2})^{1/3}\left[(1+a^\star)^{1/3} + (1-a^\star)^{1/3}\right], \tag{2}$$

$$Z_2 = \left[3a^{\star 2} + Z_1^2\right]^{1/2}, \tag{3}$$

where the $\mp$ sign indicates prograde and retrograde orbits, respectively. We will assume that the binary orbits in the same direction as the BH spin and thus take the minus sign in equation 1. Disk and BH are assumed to be coupled via strong magnetic fields and MHD turbulence in the disk is assumed to be driven through this coupling. The inner disk near the ISCO is expected to be neutrino cooled and very thin. Further out, at $r_0 + R_{\rm ISCO}$ (where $r_0 = 100$ km may be reasonable), the disk is a thick torus. We assume that turbulence in the torus leads to two overdense regions (which, in itself, is unlikely, since turbulent power will cascade to small scales) with masses $M_1 = M_2 = \epsilon M_{\rm disk}$. $\epsilon \approx 0.01 - 0.5$ (the latter is very unlikely). These two 'clumps' form a 'binary' with separation $2(r_0 + R_{\rm ISCO})$ that efficiently emits GWs and would normally lose J by GW emission, leading to inspiral. The BH is located at the center of our coordinate system and each of the clumps is located at a distance $r_0 + R_{\rm ISCO}$ from the BH. Here, following van Putten,

we assume that the lost energy and angular momentum is replenished by coupling to the central BH, so the BH loses J and spin energy. This leads to an incremental change of $R_{\rm ISCO}$ and, consequentially, of the binary separation $2(r_0 + R_{\rm ISCO})$.

2.1 Gravitational Wave Emission using the Newtonian Binary Approximation

We assume, without loss of generality, that the BH angular momentum is oriented in the $+z$-direction. Two overdense regions in the torus are approximated as point masses M_1 and M_2, where we assume $m = M_1 = M_2$. The two point masses orbit the BH at the origin in the xy-plane with angular velocity Ω. The orbital radius is $d \equiv r_0 + R_{\rm ISCO}$. We can compute the reduced mass quadrupole momentum of the system, defined as

$$I_{ij} = m \sum_A (x_{Ai} x_{Aj} - \frac{1}{3}\delta_{ij} d^2), \tag{4}$$

where A is an index denoting overdense regions. Assuming that fragment 1 sits on the positive x axis at $t = 0$, the time-dependent positions (x_i, y_i) of the two fragments are described by

$$\begin{array}{rclcrcl} x_1 &=& d\cos(\Omega t)\ , & & x_2 &=& -d\cos(\Omega t)\ , \\ y_1 &=& d\sin(\Omega t)\ , & & y_2 &=& -d\sin(\Omega t)\ . \end{array} \tag{5}$$

The quadrupole moment components we are interested in are I_{xx}, I_{xy}, and I_{yy}. Because of symmetry, $I_{xy} = I_{yx}$. Using eq. (4), we have

$$\begin{aligned} I_{xx} &= m(x_1^2 + x_2^2 - \frac{2}{3}d^2)\ , \\ &= 2md^2\cos^2\Omega t - \frac{2}{3}d^2\ , \\ &= md^2\cos 2\Omega t + const. \end{aligned} \tag{6}$$

Similiarly, we obtain the remaining components:

$$I_{ij} = md^2 \begin{pmatrix} \cos 2\Omega t + const. & \sin 2\Omega t + const \\ \sin 2\Omega t + const. & -\cos 2\Omega t + const. \end{pmatrix}, \tag{7}$$

$$\ddot{I}_{ij} = 4md^2\Omega^2 \begin{pmatrix} -\cos 2\Omega t & -\sin 2\Omega t \\ -\sin 2\Omega t & \cos 2\Omega t \end{pmatrix}, \tag{8}$$

$$\dddot{I}_{ij} = 8md^2\Omega^3 \begin{pmatrix} \sin 2\Omega t & -\cos 2\Omega t \\ -\cos 2\Omega t & -\sin 2\Omega t \end{pmatrix}. \tag{9}$$

The gravitational wave signal emitted by the binary system and the change in angular momentum and energy are given by

$$h_{ij}^{TT} = \frac{2}{D}\frac{G}{c^4}\ddot{I}_{kl}^{TT}\ , \qquad \frac{dJ_i}{dt} = -\frac{2}{5}\frac{G}{c^5}\epsilon_{ijk}\langle \ddot{I}_{jm}\dddot{I}_{mk}\rangle\ , \qquad \frac{dE}{dt} = -\frac{1}{5}\frac{G}{c^5}\langle \dddot{I}_{jk}\dddot{I}_{jk}\rangle\ . \tag{10}$$

The change of orbital energy and angular moment straightforwardly evaluate to

$$\frac{dJ_{\rm GW}}{dt} = -\frac{128}{5}\frac{G}{c^5}m^2d^4\Omega^5\ , \tag{11}$$

$$\frac{dE_{\rm GW}}{dt} = P_{\rm GW} = -\frac{128}{5}\frac{G}{c^5}m^2d^4\Omega^6\ . \tag{12}$$

Next, we must carry out the transverse-traceless projection of $\ddot{I}$ to obtain the two GW polarizations $h+$ and $h_\times$. These depend on the position (polar angle θ azimutal angle ϕ and distance D) the observer has with respect to the source. This is done most easily by expressing the GW strain in terms of spin-weighted tensor spherical harmonics,

$$h_+ - ih_\times = \frac{1}{D}\sum_{\ell=2}^{\infty}\sum_{m=-\ell}^{\ell} H_{\ell m}(t)\,{}^{-2}Y_{\ell m}(\theta,\phi)\,. \tag{13}$$

The expansion parameters H_{lm} ($\ell = 2$ denotes the quadrupole) are complex functions of the retarded source time t.
In order to express H_{2m} in terms of $\ddot{I}_{ij}$, one first expresses $h_+(\theta,\phi)$ and $h_\times(\theta,\phi)$ in terms of $\ddot{I}_{kl}$, then convolves these with ${}^{-2}Y^*_{lm}$. The result [5] is

$$H^{\rm quad}_{20} = \sqrt{\frac{32\pi}{15}}\frac{G}{c^4}\left(\ddot{I}_{zz} - \frac{1}{2}(\ddot{I}_{xx}+\ddot{I}_{yy})\right)\,, \tag{14}$$

$$H^{\rm quad}_{2\pm1} = \sqrt{\frac{16\pi}{5}}\frac{G}{c^4}\left(\mp\ddot{I}_{xz} + i\ddot{I}_{yz}\right)\,, \tag{15}$$

$$H^{\rm quad}_{2\pm2} = \sqrt{\frac{4\pi}{5}}\frac{G}{c^4}\left(\ddot{I}_{xx} - \ddot{I}_{yy} \mp 2i\ddot{I}_{xy}\right)\,. \tag{16}$$

For completeness, we give the definitions of the relevant ${}^{-2}Y^*_{lm}$:

$${}^{-2}Y_{22} = \sqrt{\frac{5}{64\pi}}(1+\cos\theta)^2 e^{2i\phi}\,, \tag{17}$$

$${}^{-2}Y_{21} = \sqrt{\frac{5}{16\pi}}\sin\theta(1+\cos\theta)e^{i\phi}\,, \tag{18}$$

$${}^{-2}Y_{20} = \sqrt{\frac{15}{32\pi}}\sin^2\theta\,, \tag{19}$$

$${}^{-2}Y_{2-1} = \sqrt{\frac{5}{16\pi}}\sin\theta(1-\cos\theta)e^{-i\phi}\,, \tag{20}$$

$${}^{-2}Y_{2-2} = \sqrt{\frac{5}{64\pi}}(1-\cos\theta)^2 e^{-2i\phi}\,. \tag{21}$$

For example, assuming the detector is located along the positive z axis ($\theta = 0, \phi = 0$), we find:

$$h_+ = \frac{1}{D}\frac{G}{c^4}(\ddot{I}_{xx} - \ddot{I}_{yy}) \tag{22}$$

$$h_\times = \frac{2}{D}\frac{G}{c^4}\ddot{I}_{xy}\,. \tag{23}$$

2.2 The coupled system of Ordinary Differential Equations

We assume that the 'binary' stays at a fixed radius. Angular momentum J lost to GW emission is provide from the BH spin. As a consequence, the BH is spun down and $R_{\rm ISCO}$ changes. We set $\dot{J}_{\rm BH} = \dot{J}_{\rm GW}$. The change in the BH mass is

$$\dot{M}_{\rm BH} = \frac{P_{\rm GW}}{c^2}, \tag{24}$$

since the gravitational mass of the BH contains the contribution due to its rotational energy. The change in $R_{\rm ISCO}$ can then be computed by differentiating equation 1,

$$\frac{dR_{\rm ISCO}}{dt} = \dot{R}_{\rm ISCO} = \left(\frac{G}{c^2}\right)\Big[\dot{M}_{\rm BH}\left(3+Z_2-\sqrt{(3-Z_1)(3+Z_1+2Z_2)}\right) + M_{\rm BH}\left(\dot{Z}_2+\frac{(Z_1+Z_2)\dot{Z}_1-(3-Z_1)\dot{Z}_2}{\sqrt{(3-Z_1)(3+Z_1+2Z_2)}}\right)\Big], \tag{25}$$

where we can express Z_1, Z_2 and their derivatives as functions of $J_{\rm BH}$, $M_{\rm BH}$, $\dot{J}_{\rm BH}$, $\dot{M}_{\rm BH}$ only,

$$\dot{Z}_1 = \frac{c\left(M_{\rm BH}\dot{J}_{\rm BH}-2J_{\rm BH}\dot{M}_{\rm BH}\right)}{3G^3M_{\rm BH}^7\left(1-a^{\star 2}\right)^{4/3}}\Big[3c^2J_{\rm BH}^2\left((1+a^\star)^{2/3}-(1-a^\star)^{2/3}\right) -2cGJ_{\rm BH}M_{\rm BH}^2\left((1+a^\star)^{2/3}+(1-a^\star)^{2/3}\right)+G^2M_{\rm BH}^4\left((1-a^\star)^{2/3}-(1+a^\star)^{2/3}\right)\Big]\ , \tag{26}$$

$$\dot{Z}_2 = \frac{3c^2J_{\rm BH}M_{\rm BH}\dot{J}_{\rm BH}-6c^2J_{\rm BH}^2\dot{M}_{\rm BH}+G^2M_{\rm BH}^5Z_1\dot{Z}_1}{G^2M_{\rm BH}^5\sqrt{\frac{3c^2J_{\rm BH}^2}{G^2M_{\rm BH}^4}+Z_1^2}}\ . \tag{27}$$

These expressions allows us to calculate the change in $R_{\rm ISCO}$ when the mass and angular momentum of the central BH change.

2.3 Application of the coupled system

At every time t, $\ddot{I}_{ij}$ and, thus, h_{ij}^{TT} depend on (*i*) the orbital radius of the 'binary', $d = r_0 + R_{\rm ISCO}$, (*ii*) the mass m of the chunks (assumed to be constant), and (*iii*) on the angular velocity, which, according to Kepler's law, we set to

$$\Omega = \sqrt{\frac{GM}{d^3}}\ . \tag{28}$$

Let us assume that the mass of the chunks forming the 'binary' is negligible with respect to the mass of the central black hole, in which case $\Omega = \sqrt{GM_{\rm BH}/(r_0+R_{\rm ISCO})^3}$. The coupled system of ODEs is then formed by equations 11, 24 and 25, with $d = r_0 + R_{\rm ISCO}$ and Ω as in equation 28. $P_{\rm GW}$ in equation 24 is given by equation 12. This system describes the evolution of $R_{\rm ISCO}, J_{\rm BH}$ and $M_{\rm BH}$. We integrate the coupled system of ODEs with a fourth-order Runge-Kutta integrator.
Note that once all spin has been extracted from the hole, the 'binary' will inspiral. However, we stop our integration when the BH is completelly spun down and do not calculate the subsequent chirp.

2.4 Astrophysically Meaningful Parameters

Mass	BH of mass $M_{\rm BH} = 5 - 10\,M_\odot$
Initial BH spin	$a^\star = 0.3 - 0.95$
Fragment mass	Assume $M_{\rm disk} = 1.5M_\odot$, $m_{\rm chunk} = \epsilon M_{\rm disk}$ with $\epsilon = 0.01 - 0.2$
Const. separation of torus from ISCO	$r_0 = 100$ km
End integration	When $J_{\rm BH} = 0$ or pre-specified run time is reached

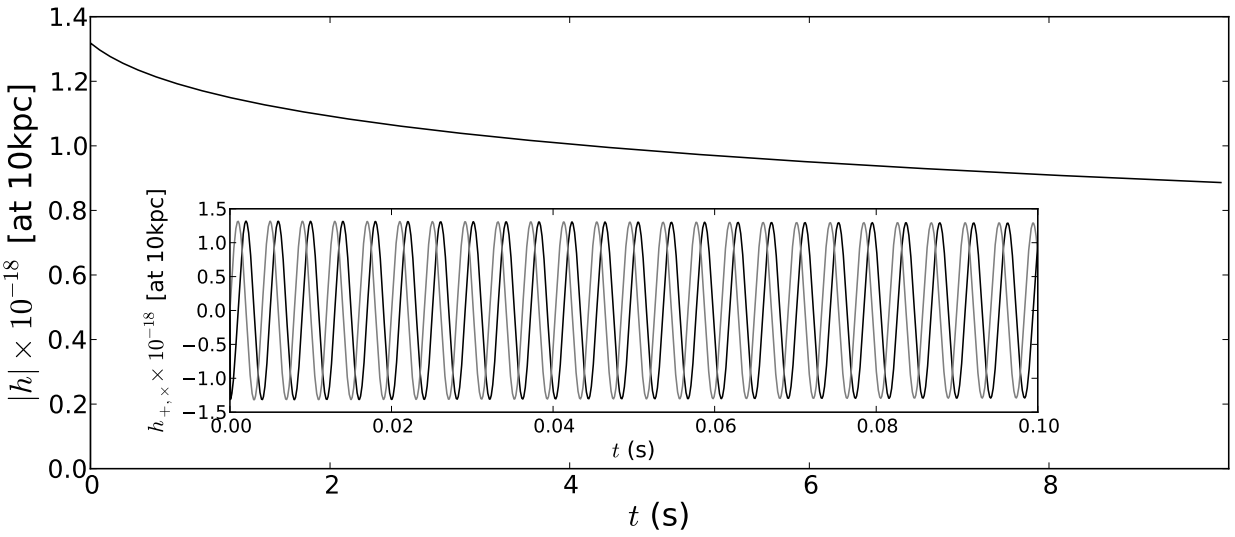

Figure 1: Waveform computed following the van Putten model. The parameters of the system are $M_{\rm BH} = 10M_\odot$, $a^\star = 0.95$, $\epsilon = 0.2$. The strain corresponds to a face-on, optimally-oriented system situated at 10 kpc. The main plot shows the absolute magnitude of the strain $|h| = \sqrt{h_+^2 + h_\times^2}$ and the inset plot shows the two polarizations zooming into the first 0.1 s of evolution.

2.5 Usage of the python script

Code usage: `$ python vanPutten.py`
The code section below `#physical parameters` allows to specify the physical parameters of the system as defined in subsection 2.4. The colatitude and azimuth of the system can be specified as well. The code section under `#parameters` allows to change the total run time (in seconds) of the integration (provided that the BH is not completely spun down, in which case the integration stops) as well as the sampling time `dt` of the output.
The script produces two output files:

- `pmvp.dat` is a diagnosis and debug output file, containing the following variables:

time	$R_{\rm ISCO}$	$J_{\rm BH}$	$M_{\rm BH}$	$a^\star$	$E_{\rm rad}$	h_+	$h_\times$

- `M*a*eps*.dat`, where the $\star$'s denote the values of the physical parameters $M_{\rm BH}$, $a^\star$ and ϵ given as input, is the production output file, containing:

time	h_+	$h_\times$

An example of the antichirp-like signal obtained for the van Putten model is shown in figure 1.

3 Torus Fragmentation Instability and Inspiral of a Single Overdense Blob

When the core-collapse supernova mechanism fails to re-energize the stalled shock (see, e.g., [6]), the protoneutron star collapses to a BH on a timescale of $\sim 500\,{\rm ms} - {\rm few\ s}$ [7]. Provided that the star has sufficient angular momentum, its collapse will eventually be halted and a massive accretion disk/torus will form around the nascent stellar-mass BH. This collapsar scenario is the leading model for long duration gamma-ray bursts and may also power an "engine driven" supernova [8].

The inner regions of the accretion disk are geometrically thin due to neutrino cooling, but the outer parts are unable to cool efficiently causing them to be thick. This potentially leads to fragmentation at large radii. We investigate the expected gravitational radiation from such a system, inspired by the discussion by Piro & Pfahl [3].

We assume a central BH of mass $M_{\rm BH}$ surrounded by a Keplerian accretion disk with orbital frequency $\Omega_{\rm disk} = (GM_{\rm BH}/r^3)^{1/2}$ and vertical scale height H. The accretion rate is $\dot{M} = 3\pi\nu\Sigma$, where Σ is the disk's surface density, $\nu = \alpha c_S H$ the usual α-viscosity prescription and c_s the isothermal speed of sound. We assume that $H/r = \eta$ is a fixed parameter.

3.1 Gravitationaly instability and fragmentation

Gravitational instability arises when

$$Q \equiv \frac{\Omega_{\rm disk} c_s}{\pi G \Sigma} < Q_{\rm crit} \simeq 1 \ . \tag{29}$$

Even once a disk becomes gravitationally unstable, numerical simulations demonstrate that fragmentation is only promoted if there is a sufficiently rapid cooling mechanism available to allow collapse to high densities. Piro & Pfahl [3] argue that photodisintegration of ^{4}He naturally leads to fragmentation because this endothermic reaction removes energy at a rate that far exceeds the viscous dissipation in the disk. In addition, the photodisintegration is very temperature sensitive and sets a clear radius were it first becomes active at around 100 gravitational radii ($R_g = GM/(rc^2)$). As explained in [3], we can therefore identify the quantity $(QH)^2\Sigma$ with the mass of the bound fragment, which is estimated to be

$$M_f \approx 0.2 \left(\frac{\eta}{0.5}\right)^3 \frac{M_{\rm BH}}{3} \ . \tag{30}$$

3.2 Migration and associated gravitational waves

Due to it's relatively large mass in comparison to surrounding disk material, the fragment accretes material within a tidal radius of itself and opens a gap in the accretion disk. It then migrates inward toward the central BH due to tidal interactions with the edges of the viscously accreting disk in a well-known process called Type II migration. (This is opposed to Type I migration, which takes places when a fragment is too small to open a gap and instead migrates inward via the generation of density waves in the disk.) This viscous migration happens on the approximate viscous timescale given by Piro & Pfahl [3],

$$t_\nu \approx \frac{1}{\alpha\eta^2\Omega} \ . \tag{31}$$

Note that since the mass of the fragment is not necessarily negligible, we use here $\Omega = \sqrt{G(M_{\rm BH}+M_f)r^{-3}}$, whereas $\Omega_{\rm disk} = \sqrt{GM_{\rm BH}r^{-3}}$.
Since the fragment-BH system is effectively a binary, there is associated GW emission that can also contribute to the inward migration of the fragment. The timescale for this can be estimated to first order via the quadrupole formula to be

$$t_{\rm GW} = \frac{5}{64\Omega}\left(\frac{G\mathcal{M}\Omega}{c^3}\right)^{-5/3} , \tag{32}$$

where $\mathcal{M} = \mu^{3/5}(M_{\rm BH}+M_f)^{2/5})$ is the chirp mass and $\mu = M_{\rm BH}M_f/(M_{\rm BH}+M_f)$ is the reduced mass of the system. The evolution of the orbit under the influence of both GW and viscous effects can be computed

by simply solving the differential equation

$$\frac{dr}{dt} = -r\left(\frac{1}{t_{\rm GW}} + \frac{1}{t_v}\right) \ , \tag{33}$$

Generally the viscous processes dominate in causing migration at large radii, while GW emission dominates at small radii. Together this leads to a unique GW signature from the fragment-BH system. This may allow the physics of the disk to be probed via the GW signal by identifying when the inspiral switches from being predominantly controlled by viscosity to being controlled by GWs.

We integrate Eq. (33) with a standard fourth-order Runge-Kutta integrator. The chirp-like gravitational wave emission expected from the system via the quadrupole approximation as discussed in the next subsection.

3.3 Gravitational Wave Signal

As in §2.1, we consider two point masses, $M_{\rm BH}$ and M_f, separated by distance r. The total mass is $M = M_{\rm BH} + M_f$ and the reduced mass is $\mu = M_{\rm BH}M_f/M$. The motion (arbitrarily assumed to be in the $x-y$ plane) of the two masses about their center of mass (at the origin) is described by the following equations:

$$\begin{aligned} x_{\rm BH} &= \frac{M_{\rm BH}}{M} r\cos(\Omega t) \ , & x_f &= -\frac{M_f}{M} r\cos(\Omega t) \ , \\ y_{\rm BH} &= \frac{M_{\rm BH}}{M} r\sin(\Omega t) \ , & y_f &= -\frac{M_f}{M} r\sin(\Omega t) \ . \end{aligned} \tag{34}$$

Here, $\Omega = \sqrt{G(M_{\rm BH}+M_f)r^{-3}}$. Now, using Eq. (4), we have

$$I_{ij} = \frac{\mu}{2} r^2 \begin{pmatrix} \cos 2\Omega t + const. & \sin 2\Omega t + const \\ \sin 2\Omega t + const. & -\cos 2\Omega t + const. \end{pmatrix}, \tag{35}$$

$$\ddot{I}_{ij} = 2\mu r^2\Omega^2 \begin{pmatrix} -\cos 2\Omega t & -\sin 2\Omega t \\ -\sin 2\Omega t & \cos 2\Omega t \end{pmatrix} \ , \tag{36}$$

$$\dddot{I}_{ij} = 4\mu r^2\Omega^3 \begin{pmatrix} \sin 2\Omega t & -\cos 2\Omega t \\ -\cos 2\Omega t & -\sin 2\Omega t \end{pmatrix} \ . \tag{37}$$

The source-angle-dependent h_+ and $h_\times$ GW polarizations can then be obtained via Eqs. (14–16).

3.4 Astrophysically Meaningful Parameters

Mass	BH of mass $M_{\rm BH} = 3 - 10 M_\odot$
Viscosity	Standard value of $\alpha = 0.1$ [3]
Geometrical parameter	$\eta = 0.3 - 0.6$ [3]
Mass of the bound fragment	The approximate factor 0.2 in Eq. (30) can be varied from $0.2 - 0.5$.
Starting Radius	Start at $r = 100 r_g$, where $r_g = \frac{GM}{c^2}$ is the gravitational radius
	End integration close to the ISCO

3.5 Usage of the python script

Code usage: `$ python pirogw.py`
The code section below `#physical parameters` allows to specify the physical parameters of the system as defined in subsection 3.4. The colatitude and azimuth of the system can be specified as well. The code

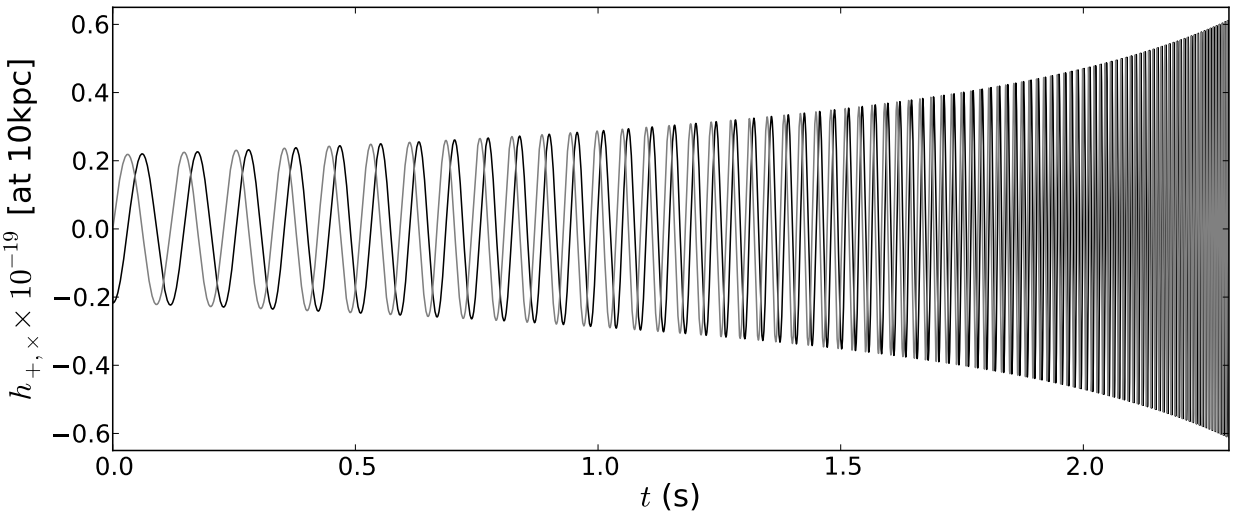

Figure 2: Waveform computed following the Piro & Pfahl model. The parameters of the system are $M_{\rm BH} = 8M_\odot$, $\eta = 0.3$, factor for the mass of the bound fragment = 0.2. The strain corresponds to a face-on, optimally-oriented system situated at 10 kpc.

section under `#parameters` allows to change the total run time (in seconds) of the integration (provided that the orbital radius is larger than $2.5R_{\rm ISCO}$ where we take a multiple of the ISCO radius of a non-spinning black hole $R_{\rm ISCO} = 6GM_{\rm BH}/c^2$ as a limit for the integration) as well as the sampling time `dt` of the output. The script produces two output files:

- `piro.dat` is a diagnosis and debug output file, containing the following variables:
time	$r\,(\mathrm{cm})$	$r\,(r_S)$	h_+	$h_\times$	Ω	t_{GW}	t_v
- `piroM*eta*fac*.dat`, where $\star$ denote the values of the physical parameters $M_{\rm BH}$, η and the factor in the RHS of equation 30 given as input, is the production output file, containing:
time	h_+	$h_\times$

An example of the chirp-like signal obtained for the Piro & Pfahl model is shown in figure 2.

4 Changes to this Document

T1100093-v2, update by C. D. Ott

- Added more details on the quadrupole approximation used in section 2.1.
- Added a caveat regarding the van Putten waveforms.
- Removed duplicate text at the end of section 3.
- Updated most of the text in section 3 based on input from Tony Piro.
- Improved description of how the gravitational wave signal is calculated for the Piro & Pfahl model.
- Updated text and `pirogw.py` script (now version 2) to correct a slight inconsistency in calculating the orbital angular velocity. Previously only the black hole mass was taken into account. Now the total system mass $M_{\rm BH} + M_f$ is used.

Acknowledgements

We thank Peter Kalmus for helpful discussions, Tony Piro for helpful suggestions, and Eric Thrane and Sarah Gossan for checking the calculations.

References

[1] M. H. van Putten, A. Levinson, H. K. Lee, T. Regimbau, M. Punturo, and G. M. Harry. *Phys. Rev. D.*, **69(4)**, 044007, 2004.

[2] M. H. van Putten. *Phys. Rev. Lett.*, **87(9)**, 091101, 2001.

[3] A. L. Piro and E. Pfahl. *Astrophys. J.*, **658**, 1173–1176, 2007.

[4] J. M. Bardeen, W. H. Press, and S. A. Teukolsky. *Astrophys. J.*, **178**, 347, 1972.

[5] P. Ajith, M. Boyle, D. A. Brown, S. Fairhurst, M. Hannam, I. Hinder, S. Husa, B. Krishnan, R. A. Mercer, F. Ohme, C. D. Ott, J. S. Read, L. Santamaria, and J. T. Whelan. *arXiv:0709.0093v3*, 2007.

[6] H.-T. Janka, K. Langanke, A. Marek, G. Martínez-Pinedo, and B. Müller. *Phys. Rep.*, **442**, 38, 2007.

[7] E. O'Connor and C. D. Ott. *Astrophys. J.*, **730**, 70, 2011.

[8] S. E. Woosley and J. S. Bloom. *Ann. Rev. Astron. Astrophys.*, **44**, 507, 2006.